Electronic Supplementary Information: Computational Investigation of van der Waals Corrections in the Adsorption Properties of Molecules on the Cu(111) Surface

Eduardo O. Bartaquim,*,† Raquel C. Bezerra,*,‡ Albert F. B. Bittencourt,*,¶ and Juarez L. F. Da Silva*,†

†*São Carlos Institute of Chemistry, University of São Paulo, P.O. Box* 780, 13560-970, *São Carlos, SP, Brazil*

‡*Secretaria de Estado de Educação e Qualidade do Ensino (SEDUC) do Estado do Amazonas, Escola Áurea Pinheiro Braga Av. Perimentral, s/n, Lot. Cidade do Leste, Gilberto Mestrinho,* 69089-340, *Manaus, AM, Brazil*

¶*School of Chemical Engineering, University of Campinas,* 13083-970, *Campinas, SP, Brazil*

E-mail: eduardoorlando34@gmail.com; racosbez@gmail.com; albertbittenc@gmail.com; juarez_dasilva@iqsc.usp.br

Contents

S1 Introduction **S-2**

S2 Selected van der Waals Corrections for DFT-PBE Calculations **S-3**

S2.1 Grimme D2 . . . . . S-4

S2.2 Grimme D3 and D3(BJ) S-5

S2.3 Tkatchenko–Scheffler S-6

S2.4 Tkatchenko–Scheffler with Iterative Hirshfeld Partitioning S-7
S2.5 Tkatchenko–Scheffler with Self-consistent Screening S-8
S2.6 Density-dependent Dispersion Correction S-9

S3 Technical Details of the PAW Projectors **S-10**

S4 Computational Convergence Tests **S-11**

S5 Equilibrium Bulk Properties **S-13**

S6 Clean Surface Properties **S-15**

S7 Gas-phase Molecules **S-19**

S8 Adsorption Properties of Molecules on the Cu(111) Surface **S-20**

References **S-25**

S1 Introduction

This document contains additional computational details employed along this work as well as complementary analyses, e.g.,

1. Section S2 summarizes additional details on the formalism of the van der Waals (vdW) corrections used in the calculations.

2. Section S3 describes the projectors chosen for the projector-augmented wave (PAW) method.

3. Section S4 provides computational convergence tests for the bulk Cu in the face-centered cubic (fcc) phase as a function of the cutoff energy and the number of **k**-points for the Brillouin integration.

4. Section S5 reports the equilibrium lattice constant, the cohesion energy, and the mechanical properties of the bulk copper. Section S6 provide additional details on the properties of the clean Cu(111) surface.

5. Section S7 contains the structural and energetic properties of the selected gas-phase molecules. Finally,

6. Section S8 summarizes specific adsorption features such as metal-molecule vertical distance, work function change, structural variations in the adsorbates, and adsorption energies.

S2 Selected van der Waals Corrections for DFT-PBE Calculations

Although density functional theory (DFT) is exact in theory,[1,2] in practice various approximations are necessary to solve the Kohn–Sham (KS) equations, especially for the exchange-correlation (XC) energy functional.[3] Local and semilocal XC energy functionals cannot provide an accurate description of the instantaneous electronic density fluctuations, which are the source of dispersion forces. Furthermore, most XC functionals only consider local properties to obtain XC energy, whereas vdW forces are derived from a non-local phenomenon.[3] The energy associated with the vdW forces is widely known to decay exponentially with $1/r^6$, where r is the interatomic separation. To account for this interaction, a common strategy is to add an energy term ($E^{\mathrm{vdW}}_{energy}$) to the total energy obtained from the DFT calculations (E^{DFT}_{tot}), i.e.,

$$E_{tot} = E^{\mathrm{DFT}}_{tot} + E^{\mathrm{vdW}}_{energy} \, . \tag{1}$$

In this study, the following vdW corrections were used in the calculations to compare their performance: (i) Grimme D2,[4] (ii) Grimme D3,[5,6] (iii) Grimme D3 with Becke–Jonson dumping factor (denoted as D3(BJ)),[7] (iv) Tkatchenko–Scheffler (TS),[8] (v) Tkatchenko–Scheffler with Self-consistent screening (TS+SCS),[9] (vi) Tkatchenko–Scheffler with iterative Hirshfeld partitioning (TS+HI),[10,11] and (vii) density-dependent dispersion correction (dDsC).[12,13] The vdW energy for all corrections takes the following form,

$$E^{\mathrm{vdW}}_{energy} = \sum_{AB} \sum_{n=6,8} s_n \frac{C^{AB}_n}{R^n_{AB}} f_{d,n}(R_{AB}) \, , \tag{2}$$

where C_n^{AB} is the dispersion coefficient, R_{AB}^n is the distance between atoms A and B, $f_{d,n}(R_{AB})$ is a dumping function required to avoid divergence when the value of R_{AB}^n is small, and s_n is a global scaling factor. The main difference between the schemes chosen for this study is found in the terms C_n^{AB} and $f_{d,n}(R_{AB})$. In the next sections, these distinctions will be examined.

S2.1 Grimme D2

Grimme's D2 approach[4] is a semi-empirical method where the dispersion coefficient has the form,

$$C_6^{AB} = \sqrt{C_6^A C_6^B}\,, \tag{3}$$

with

$$C_6^A = 0.05 N I_p^A \alpha^A\,, \tag{4}$$

where I_p^A and α^A are, respectively, the ionization potential and static dipole polarizabilities obtained with DFT-PBE0.[14] The quantity N assumes the values of 2, 10, 18, 36 and 54 for the first five periods of the periodic table. When PBE is employed, the global scaling factor takes the value of 0.75 and the damping function is provided by a Fermi-like equation:

$$f_{d,n}(R_{AB}) = \frac{1}{1 + e^{-d(R_{AB}/R_r)-1}}\,, \tag{5}$$

in which d controls the damping region and R_r represents the sum of the atomic vdW radii. The key problem with the D2 approach is the dispersion coefficient, which does not take into account variations in the chemical environment; the value remains the same regardless of variations in hybridization or oxidation state. To overcome this problem, the methods D3, TS, and dDsC were proposed.[5,6,8,10,11]

S2.2 Grimme D3 and D3(BJ)

In Grimme's D3 scheme, the dispersion coefficient is calculated using the Casimir–Polder equation,[15] which is defined as,

$$C_6^{AB} = \frac{3}{\pi}\int_0^{\infty} \alpha_A(i\omega)\alpha_B(i\omega)d\omega \,, \tag{6}$$

in which α depends on imaginary frequencies. The global scaling factor is now only adjusted when $n > 6$. In this scheme, the vdW energy is the sum of the two-body component of Equation 2 and the Axilrod–Teller–Muto triple-dipole term,[16,17] which is provided by,

$$E^{(3)} = \gamma \sum_{ABC} f_{d,3}(\overline{R}_{ABC}) \frac{C_9^{ABC}}{(R_{AB}R_{AC}R_{BC})^3} \,, \tag{7}$$

where γ is a constant that depends on the angles of the triangle $\triangle R_{AB}R_{AC}R_{BC}$ and the ternary dispersion coefficient C_9^{ABC}, which is defined as,

$$C_9^{ABC} \approx -\sqrt{C_6^{AB}C_6^{AC}C_6^{BC}} \,. \tag{8}$$

In the D3 dispersion correction, the chemical environment is taken into account using the coordination number of the atoms, more precisely the fractional coordination number,[6] which for a given atom A is defined as,

$$CN^A = \sum_{B\neq A}^{N_{at}} \frac{1}{1+e^{-k_1(k_2(R_{A,cov}+R_{B,cov})/r_{AB}-1)}} \,, \tag{9}$$

where N_{at} is the number of atoms in the chemical system, $R_{A,cov}$ and $R_{B,cov}$ are the scaled covalent radius of atoms A and B, respectively, and k_1 and k_2 are parameters with values of 16 and $4/3$. Reference molecules are now used to determine the values of $\alpha_A(i\omega)$, while the dispersion coefficients for pairs of atoms in various chemical environments ($C_{6,ref}^{AB}$) can be obtained using Equation 6. Finally, the coefficients are employed as support points in an

interpolation procedure based on the following equations:

$$C_6^{AB}(CN^A, CN^B) = \frac{Z}{W} \,, \tag{10}$$

$$Z = \sum_i^{N_A} \sum_j^{N_B} C_{6,ref}^{AB}(CN_i^A, CN_j^B) L_{ij} \,, \tag{11}$$

$$W = \sum_i^{N_A} \sum_j^{N_B} L_{ij} \,, \tag{12}$$

$$L_{ij} = e^{-k_3\left[(CN^A - CN_i^A)^2 + (CN^B - CN_j^B)^2\right]} \,, \tag{13}$$

where N_A and N_B are the number of supporting points for atoms A and B, CN_i^A and CN_j^B are the coordination numbers for the atoms in the reference systems i and j. Another essential factor is the damping function. When the distance between the atoms is small, the damping function can be zero or a finite number; in the former case, the function is a zero-damping function, while in the latter case, the function is a finite damping function. The original D3 scheme employs a zero-damping function proposed by Chai et al.[5] however, this function can be replaced by a finite damping function proposed by Grimme et al., resulting in the D3(BJ) vdW correction.[7]

S2.3 Tkatchenko–Scheffler

In the case of the TS method,[8] the parameters C_n^{AB} and $f_{d,n}$ are charge density-dependent. The dispersion coefficient is calculated as follows,

$$C_6^{AB} = \frac{2C_6^{AA}C_6^{BB}}{\frac{\alpha_0^B}{\alpha_0^A}C_6^{AA} + \frac{\alpha_0^A}{\alpha_0^B}C_6^{BB}} \,, \tag{14}$$

where:

$$\alpha_A = \frac{V_{eff}^A}{V_{free}^A}\alpha_A^{free} \,, \tag{15}$$

$$C_6^{AA} = \left(\frac{V_{eff}^A}{V_{free}^A}\right)^2 C_{6AA}^{free} \,, \tag{16}$$

in which α_A^{free} is the free-atom polarization, and V_{eff}^A and V_{free}^A correspond to the volume of atom A within a molecule and its volume as an isolated atom, respectively.

The division of V_{eff}^A by V_{free}^A represents the point in the TS method where the dependence on the chemical environment is introduced and is given by,

$$\frac{V_{eff}^A}{V_{free}^A} = \frac{\int r^3 w_A(\mathbf{r}) \rho(\mathbf{r}) d^3\mathbf{r}}{\int r^3 \rho_A^{free}(\mathbf{r}) d^3(\mathbf{r})} , \tag{17}$$

where $\rho_A^{free}(\mathbf{r})$ is the spherically averaged electron density of the neutral free atomic species and $w_A(\mathbf{r})$ is the Hirshfeld weight, which is calculated as,

$$w_A(\mathbf{r}) = \frac{\rho_A^{\text{free}}(\mathbf{r})}{\sum_B \rho_B^{free}(\mathbf{r})} . \tag{18}$$

Finally, the damping function takes the form of a Fermi-like equation:

$$f_{d,n}(R_{AB}, R_{AB}^0) = \frac{1}{1 + exp\left[-d\left(\frac{R_{AB}}{s_r R_{AB}^0} - 1\right)\right]} , \tag{19}$$

where:

$$R_{AB}^0 = R_A^0 + R_B^0 , \tag{20}$$

and

$$R_A^0 = \left(\frac{\alpha_{eff}^A}{\alpha_{free}^A}\right)^{1/3} R_A^{free} . \tag{21}$$

S2.4 Tkatchenko–Scheffler with Iterative Hirshfeld Partitioning

The Tkatchenko–Scheffler approach has certain significant limitations, such as failing when electrostatic interactions and dispersion effects become both relevant. This occurs because Hirshfeld partitioning uses neutral atoms as a reference system to determine the effective volume of atoms in a molecule. Consequently, the electronic density of the atoms within a molecule will be similar to that of the isolated atoms. This is not an issue for systems such as molecular solids or layered crystals, but for ionic solids, issues may arise.[10,11] In TS+HI approach, this problem

is addressed by overriding the Hirshfeld weight function (Equation 18) by the Hirshfeld iterative algorithm.[18] The reference system consists of fractionally charged ions generated by an iterative approach that begins with the selection of a promolecular electron density, which is determined by neutral atoms that do not interact.

The Hirshfeld weight function for step i is then calculated using the following equations,

$$w_A^i(\mathbf{r}) = \frac{\rho_A^i(\mathbf{r})}{\sum \rho_B^i(\mathbf{r})} \,. \tag{22}$$

The number of electrons in step ii is defined by the following:

$$N_A^{i+1} = N_A^i + \int \left[\rho_A^i(\mathbf{r}) - w_A^i(\mathbf{r})\rho(\mathbf{r})\right] d^3\mathbf{r} \,, \tag{23}$$

then, the charge density of the reference system becomes:

$$\rho_A^{i+1}(\mathbf{r}) = \rho^{lint(N_A^i)}(\mathbf{r}) \left[uint(N_i^A) - N_i^A\right] + \rho^{uint(N_A^i)}(\mathbf{r}) \left[N_i^A - lint(N_i^A)\right] \,, \tag{24}$$

where $lint(N_i^A)$ represents the integer part of N_i^A and $uint(N_i^A) = lint(N_i^A) + 1$. The method is repeated until the difference between the two iterative steps meets the requirement of $\Delta_A^i = |N_i^A - N_{i+1}^A|$.

S2.5 Tkatchenko–Scheffler with Self-consistent Screening

Another drawback of the TS approach is related to the screening effects. The method only considers pair-to-pair atom interactions, ignoring the influence of other atoms on this interaction; however, this is not the case in real systems. In the TS+SCS approach this problem is handled using the self-consistent screening equation to obtain the polarizabilities,

$$\alpha_A^{SCS}(\omega) = \alpha_A(\omega) - \alpha_A(\omega) \sum_{A \neq B} \tau_{AB} \alpha_B^{SCS}(\omega) \,. \tag{25}$$

In this situation, τ_{AB} is the dipole-dipole interaction tensor and α_A is defined by the following:

$$\alpha_A(w) = \frac{\alpha_A}{1 + \left(\frac{w}{w_A}\right)^2} . \tag{26}$$

The characteristic mean excitation frequency (w_A) is given by:

$$\omega_A = \frac{4}{3}\frac{C_6^{AA}}{(\alpha_A)^2} , \tag{27}$$

where the dispersion coefficient is given by the Casimir–Polder equation.

S2.6 Density-dependent Dispersion Correction

Finally, the dDsC scheme proposed by Steinmann et al. also considers the influence of the chemical environment.[12,13] In this approach, the vdW energy is based on the Becke et al. simplified exchange-hole dipole moment formalism,[19]

$$E_{energy}^{\mathrm{vdW}} = -\sum_{A=2}^{N_{At}} \sum_{B=1}^{A-1} \sum_{n=3}^{n=5} f_{2n}(bR_{AB}) \frac{C_{2n}^{AB}}{R_{AB}^{2n}} . \tag{28}$$

The dDsC correction is calculated using Equation 28 only when n is truncated in 3; otherwise, the dDsC10 scheme is used. The universal damping function f_{2n} is given by the following equation,

$$f_{2n}(x) = 1 - exp(-x) \sum_{2n}^{k=0} \frac{x^k}{k!} . \tag{29}$$

The parameter b is the Tang and Tonnies (TT) damping factor:[20]

$$b(x) = F(x) b_{AB,asym} , \tag{30}$$

where $b_{AB,asym}$ is obtained by the following combination rule:

$$b_{AB,asym} = 2\frac{b_{AA,asym} b_{BB,asym}}{b_{AA,asym} + b_{BB,asym}} . \tag{31}$$

The parameter $b_{AB,asym}$ can be estimated based on ionization energies or polarizabilities. In

the dDsC scheme, the polarizabilities are considered, then,

$$b_{AB,asym} = b_0 \sqrt[3]{\frac{1}{\alpha_i}} \,, \tag{32}$$

in which α_i is defined in Equation 15 and b_0 is a parameter related to the strength of the correction in the medium range. Furthermore, $F(x)$ is given by,

$$F(X) = \frac{2}{e^{a_0 x} + 1} \,, \tag{33}$$

where a_0 is a fitted parameter that controls short-range behavior, while x is the damping argument defined by:

$$x = \left(2q_{AB} + \frac{abs((Z_A - N_A^D)(Z_B - N_A^D))}{r_{AB}} \right) \frac{N_A^D + N_B^D}{N_A^D N_B^D} \,, \tag{34}$$

in which Z_A denotes the nuclear charge, N_A^D is the Hirshfield dominantion population, and the term $2q_{AB} = q_{AA} + q_{AB}$ denotes a covalent band index based on the overlap of conventional Hirshfeld populations:

$$q_{AB} = \int w_A(\mathbf{r}) w_B(\mathbf{r}) \rho(\mathbf{r}) dw_i(\mathbf{r}) \,. \tag{35}$$

S3 Technical Details of the PAW Projectors

Table S1: Computational details on PAW projectors: recommended minimum and maximum cutoff energies, `ENMIN` (eV) and `ENMAX` (eV), respectively; and number of valence electrons, `ZVAL`.

Element	PAW projector	`ENMIN`	`ENMAX`	`ZVAL`	Valence electrons
Cu	PAW_PBE Cu_Gw	312.779	417.039	11	$3d^{10}4s^1$
C	PAW_PBE C_GW_new	310.494	413.992	4	$2s^2 2p^2$
H	PAW_PBE H_GW	250.000	300.000	1	$1s^1$
O	PAW_PBE O_GW_new	325.824	434.431	6	$2s^2 2p^4$

S4 Computational Convergence Tests

Table S2: Computational convergence of bulk properties of Cu in the face-centered cubic structure as a function of the plane-wave cutoff energy (ENCUT) and the **k**-mesh: Equilibrium lattice constant, as defined in Figure S3, (a_0), deviation of the lattice constant parameter in relation to the values calculated using the highest ENCUT or **k**-mesh of each convergence test set ($\Delta a_0 = 100(a_0^i - a_0^{ref})/a_0^{ref}$), total energy ($E_{tot}$), deviation in relation to values calculated using the highest ENCUT or **k**-mesh of each convergence test set ($\Delta E_{tot} = (E_{tot}^i - E_{tot}^{ref})$.

DFT	ENCUT (eV)	**k**-mesh	Number of **k**-points	a_0 (Å)	Δa_0 (%)	E_{tot} (eV)	ΔE_{tot} (meV)
PBE	417.039	14×14×14	104	3.585	−1.226	−3.744 442	3.223
	521.298	14×14×14	104	3.623	−0.170	−3.755 894	−8.229
	625.558	14×14×14	104	3.621	−0.249	−3.748 312	−0.647
	729.818	14×14×14	104	3.630	0.003	−3.747 932	−0.266
	834.078	14×14×14	104	3.630	0.004	−3.747 985	−0.320
	938.337	14×14×14	104	3.630	0.000	−3.747 665	0.000
	834.078	5×5×5	10	3.625	−0.186	−3.845 642	−96.744
	834.078	7×7×7	20	3.629	−0.064	−3.787 536	−38.638
	834.078	10×10×10	47	3.633	0.050	−3.733 210	15.688
	834.078	12×12×12	72	3.630	−0.042	−3.743 989	4.909
	834.078	14×14×14	104	3.630	−0.044	−3.747 985	0.913
	834.078	17×17×17	165	3.629	−0.071	−3.746 145	2.752
	834.078	19×19×19	220	3.629	−0.054	−3.745 342	3.556
	834.078	21×21×21	286	3.630	−0.040	−3.745 653	3.245
	834.078	24×24×24	413	3.631	0.000	−3.748 898	0.000
PBE	417.039	14×14×14	120	3.559	−1.184	−4.100 245	3.675
+	521.298	14×14×14	104	3.597	−0.133	−4.112 376	−8.456
TS+SCS	625.558	14×14×14	104	3.594	−0.210	−4.104 671	−0.751
	729.818	14×14×14	104	3.602	0.029	−4.104 213	−0.293
	834.078	14×14×14	104	3.604	0.066	−4.104 262	0.342
	938.337	14×14×14	104	3.601	0.000	−4.103 920	0.000
	834.078	5×5×5	10	3.597	−0.162	−4.202 754	−97.551
	834.078	7×7×7	20	3.602	−0.038	−4.144 004	−38.801
	834.078	10×10×10	47	3.605	0.059	−4.089 009	16.194
	834.078	12×12×12	72	3.602	−0.022	−4.100 703	4.499
	834.078	14×14×14	104	3.604	0.022	−4.104 262	0.940
	834.078	17×17×17	165	3.600	−0.073	−4.102 992	2.211
	834.078	19×19×19	220	3.602	−0.025	−4.102 058	3.145
	834.078	21×21×21	328	3.603	0.001	−4.105 345	−0.142
	834.078	24×24×24	413	3.603	0.000	−4.105 203	0.000

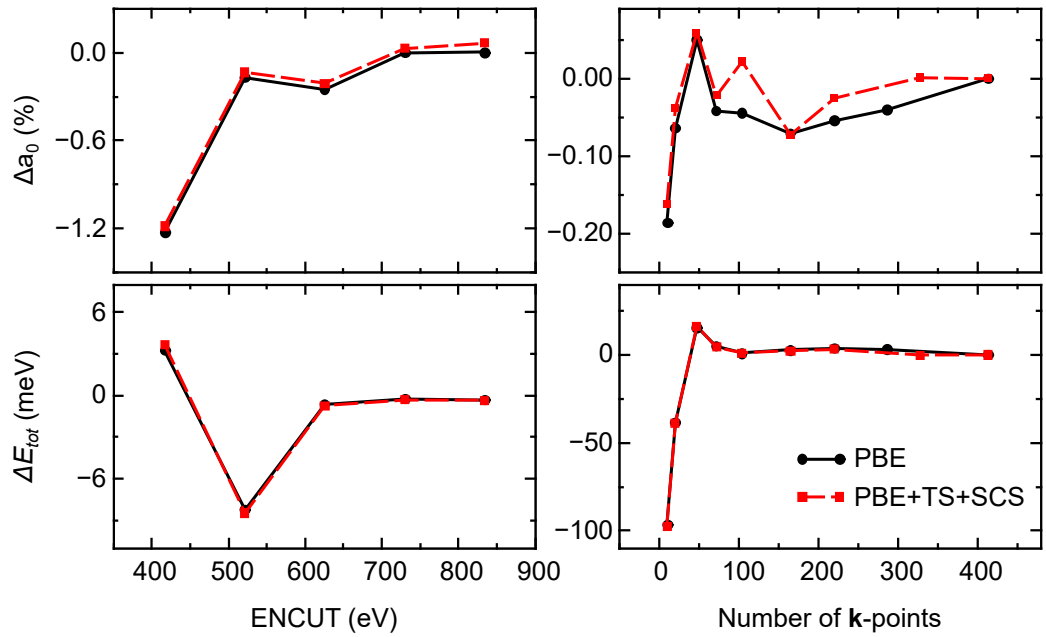

Figure S1: Computational convergence of the equilibrium lattice constant parameter (a_0) and total energy (E_{tot}) as a function of the plane-wave cutoff energy (`ENCUT`) and the number of **k**-points in the irreducible part of the Brillouin zone.

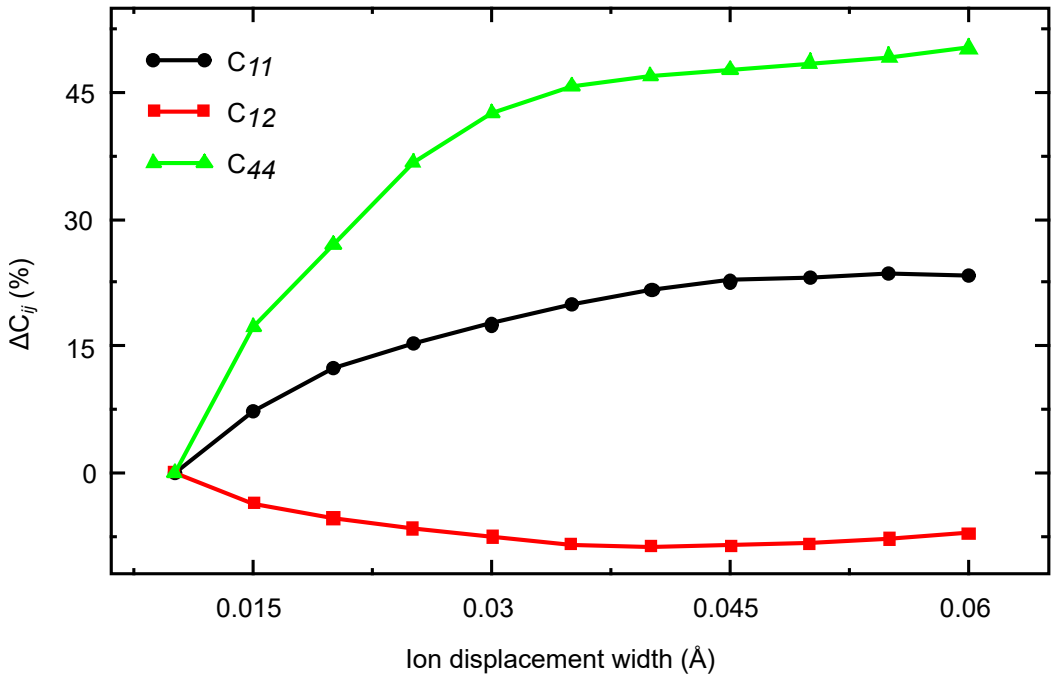

Figure S2: Computational convergence of the bulk Cu elastic constants (C_{11}, C_{12}, and C_{44}) with respect to the ion displacement width. All ΔC_{ij} values were calculated with respect to the elastic constant calculated using the smallest ion displacement width (0.010 Å), i.e., $\Delta C_{ij} = 100(C_{ij}^{k} - C_{ij}^{ref})/C_{ij}^{ref}$.

S5 Equilibrium Bulk Properties

Table S3: Effect of the vdW corrections on the bulk properties of Cu in the face-centered cubic structure: Equilibrium lattice constant (a_0), deviation from the value obtained with PBE in percentage ($\Delta a_0 = 100(a_0^i - a_0^{\mathrm{PBE}})/a_0^{\mathrm{PBE}}$), total energy ($E_{tot}$), deviation from the value obtained with PBE ($\Delta E_{tot} = (E_{tot}^i - E_{tot}^{\mathrm{PBE}})$, cohesion energy ($E_{coh}$), deviation from the value obtained with PBE in percentage ($\Delta E_{coh} = 100(E_{coh}^i - E_{coh}^{\mathrm{PBE}})/E_{coh}^{\mathrm{PBE}}$). All values were obtained using a cutoff energy of 834.078 eV and a density of **k**-points of 40 Å^{-1}.

DFT	a_0 (Å)	Δa_0 (%)	E_{tot} (eV)	ΔE_{tot} (eV)	E_{coh} (eV)	ΔE_{coh} (%)
PBE	3.630	0.00	−3.745 342	0.00	−3.502	0.00
PBE+D2	3.565	−1.77	−4.164 016	−0.42	−3.920	11.96
PBE+D3	3.563	−1.84	−4.256 797	−0.51	−4.013	14.61
PBE+D3(BJ)	3.563	−1.84	−4.338 104	−0.59	−4.094	16.93
PBE+TS	3.542	−2.41	−4.359 018	−0.61	−4.115	17.53
PBE+TS+SCS	3.602	−0.76	−4.102 058	−0.36	−3.858	10.19
PBE+TS+HI	3.544	−2.35	−4.345 918	−0.60	−4.102	17.15
PBE+dDsC	3.590	−1.08	−4.071 484	−0.33	−3.828	9.31
Expt.	3.615[21]	0.40	-	-	−3.480[22]	0.62

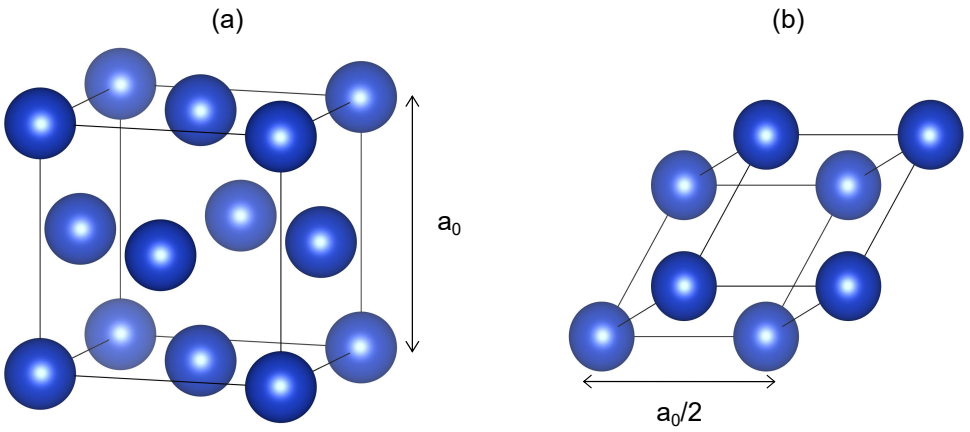

Figure S3: Molecular representation for the bulk Cu in the face-centered cubic structure: (a) conventional unit cell and (b) primitive cell. The lattice constant (a_0) is indicated by the double arrow, while the dotted lines delimit the unit cells.

Table S4: Effect of the vdW corrections on the mechanical properties of bulk Cu in the face-centered cubic structure: Elastic constants (C_{ij}), deviation from the value obtained with PBE in percentage ($\Delta C_{ij} = 100(C_{ij}^{k} - C_{ij}^{\mathrm{PBE}})/C_{ij}^{\mathrm{PBE}}$), bulk modulus ($B$), deviation from the value obtained with PBE in percentage ($\Delta B = 100(B^{k} - B^{\mathrm{PBE}})/B^{\mathrm{PBE}}$), Young's modulus ($E$), deviation from the value obtained with PBE in percentage ($\Delta E = 100(E^{k} - E^{\mathrm{PBE}})/E^{\mathrm{PBE}}$), shear modulus ($G$), and deviation from the value obtained with PBE in percentage ($\Delta G = 100(G^{k} - G^{\mathrm{PBE}})/G^{\mathrm{PBE}}$).

DFT	C_{11} (GPa)	ΔC_{11} (%)	C_{12} (GPa)	ΔC_{12} (%)	C_{44} (GPa)	ΔC_{44} (%)	B (GPa)	ΔB (%)	E (GPa)	ΔE (%)	G (GPa)	ΔG (%)
PBE	168.74	0.00	125.10	0.00	73.20	0.00	139.65	0.00	140.32	0.00	52.65	0.00
PBE+D2	180.88	7.19	136.28	8.94	83.62	14.22	151.15	8.23	156.83	11.77	59.09	12.23
PBE+D3	203.82	20.79	141.43	13.05	87.21	19.14	162.23	16.17	171.57	22.27	64.81	23.10
PBE+D3(BJ)	200.98	19.10	147.56	17.95	93.35	27.51	165.37	18.42	176.37	25.69	66.69	26.67
PBE+TS	206.31	22.26	156.26	24.90	101.42	38.54	172.94	23.84	187.04	33.30	70.86	34.59
PBE+TS+SCS	164.08	−2.76	145.28	16.13	69.18	−5.50	151.54	8.51	123.51	−11.98	45.27	−14.02
PBE+TS+HI	209.18	23.96	158.46	26.66	103.64	41.57	175.37	25.58	190.75	35.94	72.33	37.38
PBE+dDsC	190.00	12.60	141.18	12.85	84.50	15.43	157.45	12.75	160.81	14.60	60.46	14.83
Expt.	168.3[23]	−0.26	122.1[23]	−2.40	75.7[23]	3.41	142.06[24]	1.73	130[24]	−7.35	47.9[25]	−9.02

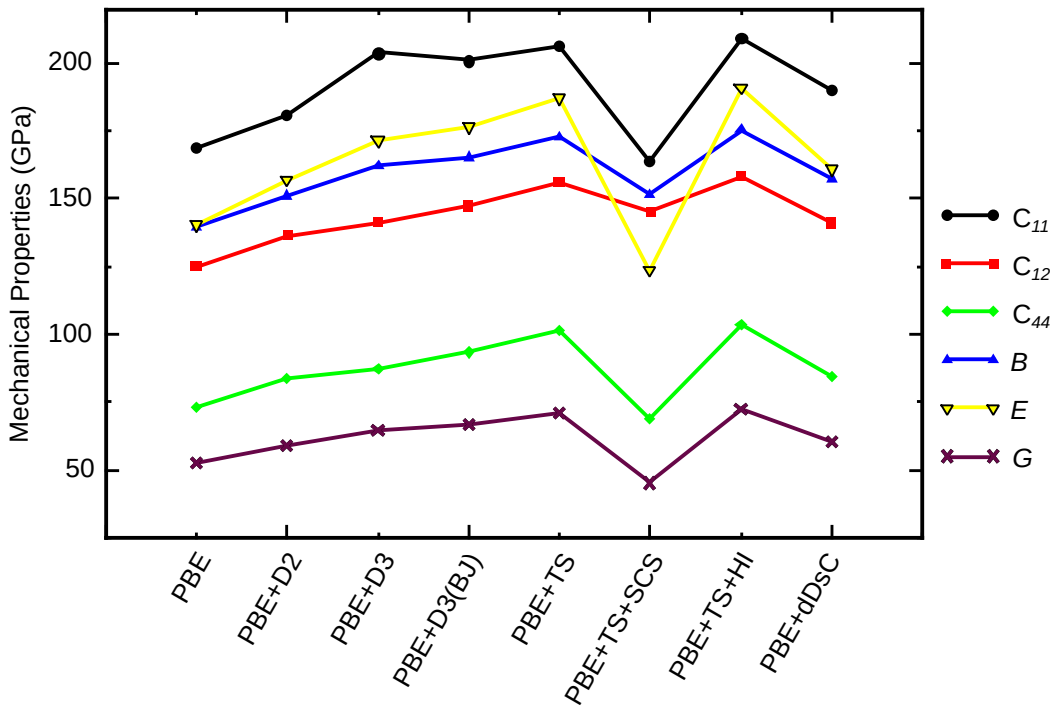

Figure S4: Effect of the vdW corrections on the mechanical properties of bulk Cu in the face-centered cubic structure: elastic constants (C_{11}, C_{12}, C_{44}), bulk modulus (B), Young's modulus (E), and shear modulus (G).

S6 Clean Surface Properties

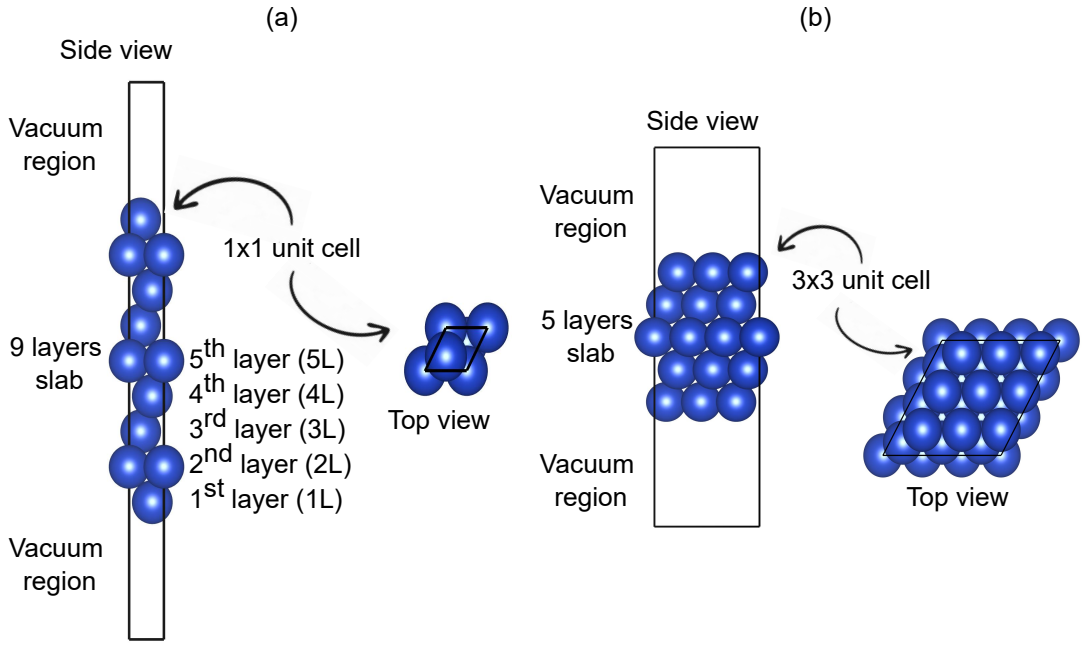

Figure S5: Molecular representation for the slab models: (a) Slab model used to evaluate the properties of the Cu(111) clean surface using a 1×1 surface unit cell with 9 layers in the slab, (b) slab model used to study the adsorption the properties of molecules on the Cu(111) surface using a 3×3 surface unit cell with 5 layers in the slab.

Table S5: Effect of the vdW corrections on the clean-surface properties of the Cu(111) surface: Surface energy per atom (σ), surface energy per area (γ), deviation from the value obtained with PBE in percentage ($\Delta\gamma = 100(\gamma^i - \gamma^{\mathrm{PBE}})/\sigma^{\mathrm{PBE}}$), work function ($\Phi$), deviation from the value obtained with PBE in percentage ($\Delta\Phi = 100(\Phi^i - \Phi^{\mathrm{PBE}})/\Phi^{\mathrm{PBE}}$).

DFT	σ^* (eV/atom)	γ^* (J/m^2)	$\Delta\gamma$ (%)	$\Phi^\dagger$ (eV)	$\Delta\Phi$ (%)
PBE	0.462	1.298	0.00	4.805	0.00
PBE+D2	0.686	1.997	53.84	4.843	0.78
PBE+D3	0.763	2.225	71.34	4.854	1.01
PBE+D3(BJ)	0.765	2.231	71.85	4.849	0.92
PBE+TS	0.868	2.559	97.10	4.857	1.07
PBE+TS+SCS	0.313	0.892	−31.34	4.806	0.02
PBE+TS+HI	0.857	2.526	94.52	4.862	1.19
PBE+dDsC	0.633	1.817	39.97	4.815	0.21
Expt.	-	1.825[26]	40.56	4.98[27]	3.64

* $\sigma = \frac{1}{2N_{tot}}(E_{tot}^{\mathrm{slab}} - N_l E_{tot}^{\mathrm{bulk}})$ and $\gamma = \frac{1}{2A}(E_{tot}^{\mathrm{slab}} - N_l E_{tot}^{\mathrm{bulk}})$, where E_{tot}^{slab} is the slab total energy, E_{tot}^{bulk} the bulk total energy, N_l is the number of layers in the slab, N_{tot} is the total number of atoms in the slab, and A is the slab area.

† $\Phi = V_{es}(\mathbf{r}_{vac}) - E_{\mathrm{Fermi}}$, where $V_{es}(\mathbf{r}_{vac})$ is the electrostatic potential in vacuum and E_{Fermi} the Fermi level.

Table S6: Effect of the vdW corrections on the clean surface properties of the Cu(111) surface: Change in the interlayer spacing upon structure optimization (d_{ij}), deviation from the value obtained with PBE in percentage ($\Delta d_{ij} = 100(\Delta d_{ij}^k - \Delta d_{ij}^{\mathrm{PBE}})/\Delta d_{ij}^{\mathrm{PBE}}$), and change in the slab volume upon structure optimization (ΔV).

DFT	Δd_{12} (%)	Δd_{12} (%)	Δd_{23} (%)	Δd_{23} (%)	Δd_{34} (%)	Δd_{34} (%)	Δd_{45} (%)	Δd_{45} (%)	ΔV (%)
PBE	−0.901	0.00	−0.293	0.00	0.076	0.00	0.278	0.00	−0.210
PBE+D2	0.442	−149.02	−0.192	−34.43	−0.136	−279.04	0.105	−62.11	0.055
PBE+D3	1.003	−211.36	−0.083	−71.61	−0.248	−427.81	0.020	−92.72	0.173
PBE+D3(BJ)	0.667	−174.02	−0.092	−68.73	−0.197	−360.37	0.063	−77.27	0.110
PBE+TS	1.579	−275.32	−0.006	−97.81	−0.288	−480.28	−0.089	−132.13	0.299
PBE+TS+SCS	−1.155	28.20	−2.267	673.69	−2.396	−3265.28	−2.433	−975.71	−2.062
PBE+TS+HI	1.478	−264.14	−0.007	−97.72	−0.266	−451.01	−0.067	−124.08	0.285
PBE+dDsC	−0.038	−95.82	−0.046	−84.45	−0.051	−167.24	0.099	−64.46	−0.009

Table S7: Effect of the vdW corrections on the d-band center (ε_d^i) for each layer i in the Cu(111) clean surface model. Values of percentage deviation ($\Delta\varepsilon_d^i$) were calculated with respect to the value obtained with PBE.

DFT	ε_d^1 (eV)	$\Delta\varepsilon_d^1$ (%)	ε_d^2 (eV)	$\Delta\varepsilon_d^2$ (%)	ε_d^3 (eV)	$\Delta\varepsilon_d^3$ (%)	ε_d^4 (eV)	$\Delta\varepsilon_d^4$ (%)	ε_d^5 (eV)	$\Delta\varepsilon_d^5$ (%)
PBE	−2.463	0.000	−2.768	0.000	−2.760	0.000	−2.761	0.000	−2.775	0.000
PBE+D2	−2.563	4.031	−2.905	4.938	−2.918	5.739	−2.924	5.904	−2.939	5.907
PBE+D3	−2.556	3.751	−2.900	4.754	−2.922	5.870	−2.931	6.158	−2.946	6.163
PBE+D3(BJ)	−2.563	4.056	−2.906	4.993	−2.923	5.917	−2.931	6.169	−2.946	6.170
PBE+TS	−2.589	5.099	−2.944	6.358	−2.976	7.822	−2.988	8.229	−3.004	8.260
PBE+TS+SCS	−2.502	1.567	−2.846	2.829	−2.891	4.750	−2.907	5.292	−2.913	4.966
PBE+TS+HI	−2.587	5.018	−2.940	6.196	−2.970	7.594	−2.982	7.994	−2.998	8.030
PBE+dDsC	−2.527	2.602	−2.850	2.966	−2.852	3.341	−2.859	3.550	−2.876	3.644

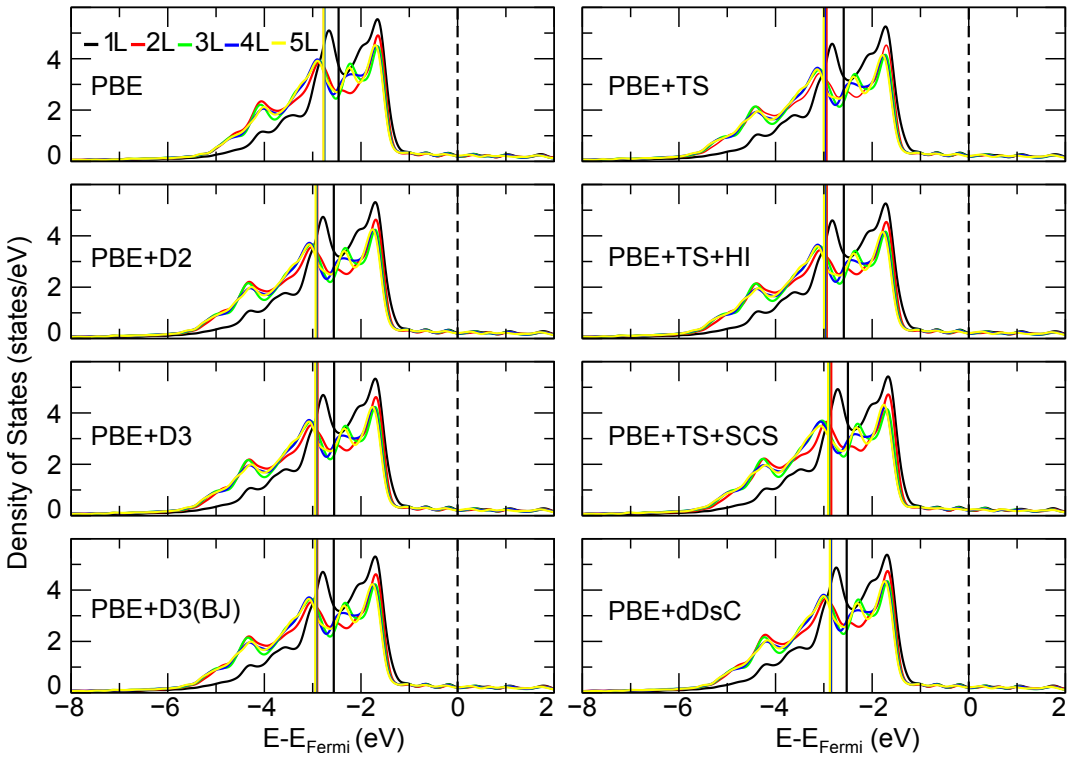

Figure S6: Density of states for the first five layers in the Cu(111) slab. The dashed line represents the Fermi level, while the vertical colored solid lines represent the d-band center for each corresponding layer.

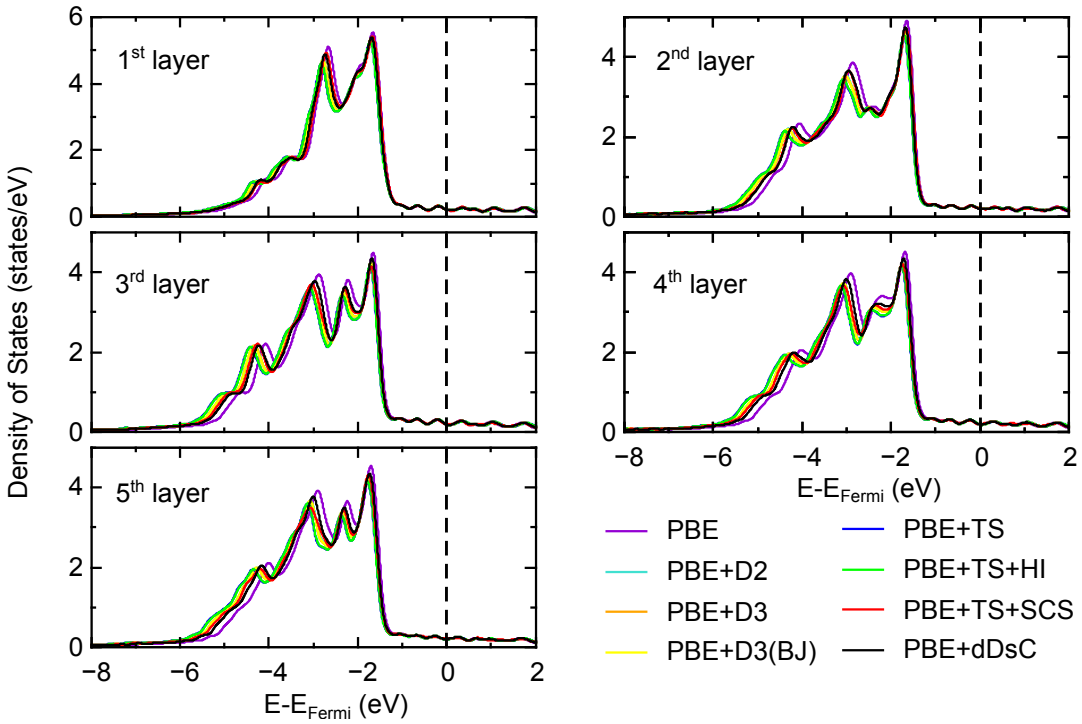

Figure S7: Effect of the vdW corrections on the density of states for the first five layers of the Cu(111) slab. Colored solid lines indicate the vdW corrections considered in this study.

S7 Gas-phase Molecules

Table S8: Effect of the vdW corrections on the properties of gas-phase molecules: Average bond length (d_b), average bond angle (α), bond energy (E_b), and energy difference between the HOMO and the LUMO orbitals (E_g). Experimental data available in Ref. 28.

Property	DFT	CH_3	CH_4	CO	CO_2	H_2O	OH
d_b (Å)	PBE	1.087	1.097	1.138	1.173	0.971	0.985
	PBE+D2	1.089	1.098	1.138	1.173	0.971	0.985
	PBE+D3	1.088	1.097	1.138	1.173	0.971	0.985
	PBE+D3(BJ)	1.087	1.097	1.138	1.173	0.971	0.985
	PBE+TS	1.087	1.097	1.138	1.173	0.971	0.985
	PBE+TS+SCS	1.087	1.097	1.138	1.173	0.971	0.985
	PBE+TS+HI	1.087	1.097	1.138	1.173	0.971	0.985
	PBE+dDsC	1.088	1.097	1.138	1.173	0.971	0.985
	Expt.	1.079	1.087	1.128	1.162	0.958	0.97
α (°)	PBE	120.0	109.5	-	180.0	104.1	-
	PBE+D2	120.0	109.5	-	180.0	104.1	-
	PBE+D3	120.0	109.5	-	180.0	104.1	-
	PBE+D3(BJ)	120.0	109.5	-	180.0	104.1	-
	PBE+TS	120.0	109.5	-	180.0	104.1	-
	PBE+TS+SCS	120.0	109.5	-	180.0	104.1	-
	PBE+TS+HI	120.0	109.5	-	180.0	104.1	-
	PBE+dDsC	120.0	109.5	-	180.0	104.1	-
	Expt.	120.0	109.5	-	180.0	104.5	-
E_b (eV)	PBE	−13.42	−18.18	−11.63	−17.99	−10.13	−4.75
	PBE+D2	−13.43	−18.20	−11.63	−18.00	−10.13	−4.75
	PBE+D3	−13.42	−18.18	−11.63	−18.00	−10.13	−4.75
	PBE+D3(BJ)	−13.44	−18.21	−11.64	−18.02	−10.14	−4.76
	PBE+TS	−13.42	−18.18	−11.63	−17.99	−10.13	−4.75
	PBE+TS+SCS	−13.42	−18.18	−11.63	−17.99	−10.13	−4.75
	PBE+TS+HI	−13.42	−18.18	−11.63	−17.99	−10.13	−4.75
	PBE+dDsC	−13.42	−18.18	−11.63	−18.01	−10.13	−4.75
	Expt.	−12.53	−17.02	−11.11	−16.56	−9.51	−4.41
E_g (eV)	PBE	4.93	8.98	6.96	8.08	6.23	6.50
	PBE+D2	4.93	8.97	6.96	8.08	6.23	6.50
	PBE+D3	4.93	8.98	6.96	8.08	6.23	6.50
	PBE+D3(BJ)	4.93	8.98	6.96	8.08	6.23	6.50
	PBE+TS	4.93	8.98	6.96	8.08	6.23	6.50
	PBE+TS+SCS	4.93	8.98	6.96	8.08	6.23	6.50
	PBE+TS+HI	4.93	8.98	6.96	8.08	6.23	6.50
	PBE+dDsC	4.93	8.98	6.96	8.08	6.23	6.50

S8 Adsorption Properties of Molecules on the Cu(111) Surface

Table S9: Effect of the vdW corrections on the properties of adsorbed systems. Distance between the Cu surface and the molecule (d_{Mol-Cu}), molecular bond length and its percentage deviation from gas-phase values (d_b) and (Δd_b), average bond angle and its percentage deviation from gas-phase values (α, $\Delta\alpha$), and the adsorption energy (E_{ad}).

Molecule	DFT	Site	d_{Mol-Cu} (Å)	d_b (Å)	Δd_b (%)	α (°)	$\Delta\alpha$ (%)	E_{ad} (eV)
CH_3	PBE	Bridge	1.791	1.107	1.82	105.9	−11.71	−1.515
		Hollow fcc	1.769	1.108	1.85	105.8	−11.82	−1.526
		Hollow hcp	1.753	1.108	1.85	105.9	−11.72	−1.519
		Top	2.189	1.097	0.92	109.6	−8.65	−1.349
		Top*	2.158	1.098	0.95	109.5	−8.78	−1.350
	PBE+D3	Bridge	1.876	1.103	1.38	107.2	−10.68	−1.802
		Hollow fcc	1.742	1.106	1.74	106.2	−11.52	−1.917
		Hollow hcp	1.727	1.106	1.74	106.4	−11.35	−1.908
		Top	2.109	1.097	0.89	109.9	−8.38	−1.702
		Top*	2.079	1.098	1.00	109.4	−8.87	−1.713
	PBE+dDsC	Bridge	1.892	1.103	1.39	107.1	−10.78	−1.618
		Hollow fcc	1.780	1.103	1.39	107.0	−10.81	−1.642
		Hollow hcp	1.746	1.107	1.79	106.1	−11.59	−1.708
		Top	2.113	1.097	0.87	109.7	−8.58	−1.533
		Top*	2.095	1.098	0.94	109.4	−8.84	−1.536
CH_4	PBE	Bridge	3.359	1.097	0.00	109.5	0.00	0.007
		Hollow fcc	3.340	1.097	0.00	109.5	0.00	0.009
		Hollow hcp	3.369	1.097	0.00	109.5	0.00	0.005
		Top	3.374	1.097	−0.01	109.5	0.00	0.007
		Top*	3.389	1.097	−0.01	109.5	0.00	0.005
	PBE+D3	Bridge	3.079	1.098	0.08	109.5	0.00	−0.276
		Hollow fcc	3.244	1.098	0.04	109.5	0.00	−0.275
		Hollow hcp	3.032	1.098	0.09	109.5	0.00	−0.272
		Top	3.053	1.098	0.07	109.5	0.00	−0.267
		Top*	3.066	1.098	0.05	109.5	0.00	−0.268
	PBE+dDsC	Bridge	3.139	1.098	0.05	109.5	0.00	−0.159
		Hollow fcc	3.134	1.098	0.04	109.5	0.00	−0.157
		Hollow hcp	3.137	1.098	0.06	109.5	0.00	−0.163
		Top	3.149	1.098	0.03	109.5	0.00	−0.157
		Top*	3.133	1.098	0.04	109.5	0.00	−0.154
CO	PBE	Bridge	1.556	1.171	2.85	-	-	−0.854
		Hollow fcc	1.482	1.178	3.47	-	-	−0.935
		Hollow hcp	1.476	1.177	3.45	-	-	−0.894

Continue on next page

Table S9: Continued from previous page.

Molecule	DFT	Site	d_{Mol-Cu} (Å)	d_b (Å)	Δd_b (%)	α (°)	$\Delta\alpha$ (%)	E_{ad} (eV)
		Top	1.959	1.152	1.19	-	-	−0.779
		Top*	1.795	1.157	1.64	-	-	−0.756
	PBE+D3	Bridge	1.555	1.170	2.84	-	-	−1.062
		Hollow fcc	1.492	1.177	3.38	-	-	−1.115
		Hollow hcp	1.479	1.176	3.36	-	-	−1.074
		Top	1.945	1.152	1.19	-	-	−0.963
		Top*	1.780	1.157	1.61	-	-	−0.958
	PBE+dDsC	Bridge	1.496	1.171	1.61	-	-	−0.980
		Hollow fcc	1.475	1.177	2.86	-	-	−1.056
		Hollow hcp	1.468	1.177	3.43	-	-	−1.019
		Top	1.941	1.152	3.41	-	-	−0.900
		Top*	1.712	1.157	1.21	-	-	−0.877
CO_2	PBE	Bridge	3.426	1.173	0.03	179.9	−0.04	−0.008
		Hollow fcc	3.443	1.173	0.03	179.9	−0.06	−0.006
		Hollow hcp	3.448	1.173	0.03	179.9	−0.06	−0.007
		Top	3.546	1.173	0.03	179.9	−0.06	−0.009
		Top*	3.510	1.173	0.04	179.9	−0.06	−0.006
	PBE+D3	Bridge	3.198	1.173	0.06	179.8	−0.13	−0.229
		Hollow fcc	3.196	1.173	0.06	179.8	−0.12	−0.227
		Hollow hcp	3.184	1.173	0.06	179.8	−0.11	−0.228
		Top	3.240	1.173	0.06	179.7	−0.14	−0.218
		Top*	3.220	1.173	0.07	179.7	−0.13	−0.219
	PBE+dDsC	Bridge	3.180	1.173	0.03	179.8	−0.11	−0.152
		Hollow fcc	3.215	1.173	0.03	179.8	−0.11	−0.150
		Hollow hcp	3.305	1.173	0.03	179.8	−0.10	−0.161
		Top	3.281	1.173	0.02	179.7	−0.15	−0.145
		Top*	3.325	1.173	0.03	179.8	−0.12	−0.151
H_2O	PBE	Bridge	2.462	0.978	0.71	104.0	−0.15	−0.175
		Hollow fcc	2.744	0.976	0.51	103.6	−0.52	−0.083
		Hollow hcp	2.447	0.978	0.73	103.9	−0.20	−0.172
		Top	2.399	0.978	0.72	104.3	0.21	−0.184
		Top*	2.463	0.977	0.61	104.6	0.47	−0.179
	PBE+D3	Bridge	2.326	0.979	0.85	103.8	−0.30	−0.422
		Hollow fcc	2.319	0.980	0.89	103.5	−0.58	−0.423
		Hollow hcp	2.317	0.979	0.87	103.7	−0.38	−0.413
		Top	2.364	0.979	0.81	104.3	0.15	−0.427
		Top*	2.330	0.978	0.73	104.5	0.32	−0.424
	PBE+dDsC	Bridge	2.308	0.979	0.80	103.9	−0.19	−0.317
		Hollow fcc	2.300	0.979	0.83	103.8	−0.31	−0.317
		Hollow hcp	2.303	0.979	0.83	103.9	−0.25	−0.304
		Top	2.360	0.978	0.71	104.4	0.24	−0.325

Continue on next page

Table S9: Continued from previous page.

Molecule	DFT	Site	d_{Mol-Cu} (Å)	d_b (Å)	Δd_b (%)	α (°)	$\Delta\alpha$ (%)	E_{ad} (eV)
		Top*	2.319	0.977	0.65	104.7	0.54	−0.328
OH	PBE	Bridge	1.366	0.972	−1.33	-	-	−3.088
		Hollow fcc	1.364	0.972	−1.31	-	-	−3.089
		Hollow hcp	1.415	0.972	−1.32	-	-	−3.009
		Top	1.897	0.966	−1.98	-	-	−2.160
		Top*	1.982	0.975	−1.08	-	-	−2.460
	PBE+D3	Bridge	1.510	0.970	−1.43	-	-	−2.983
		Hollow fcc	1.399	0.971	−1.41	-	-	−3.185
		Hollow hcp	1.449	0.971	−2.05	-	-	−3.116
		Top	1.875	0.965	−1.08	-	-	−2.280
		Top*	1.951	0.975	−1.18	-	-	−2.603
	PBE+dDsC	Bridge	1.481	0.974	−1.18	-	-	−2.974
		Hollow fcc	1.381	0.972	−1.39	-	-	−3.124
		Hollow hcp	1.428	0.971	−1.41	-	-	−3.056
		Top	1.877	0.966	−1.97	-	-	−2.229
		Top*	1.946	0.974	−1.09	-	-	−2.517

Table S10: Effect of the vdW corrections on the properties of adsorbed systems: Work function (Φ), change in the work function ($\Delta\Phi$), change in the Bader charge of the adsorbed molecule and the substrate, indicated by ΔQ_{Mol} and ΔQ_{Sub}, respectively.

	PBE				PBE+D3				PBE+dDsC			
System	Φ (eV)	$\Delta\Phi$ (eV)	ΔQ_{Mol} (e)	ΔQ_{Sub} (e)	Φ (eV)	$\Delta\Phi$ (eV)	ΔQ_{Mol} (e)	ΔQ_{Sub} (e)	Φ (eV)	$\Delta\Phi$ (eV)	ΔQ_{Mol} (e)	ΔQ_{Sub} (e)
CH_3	4.24	−0.57	−0.34	0.34	4.24	−0.62	−0.33	0.33	4.36	−0.46	−0.30	0.30
CH_4	4.61	−0.19	−0.03	0.03	4.61	−0.24	−0.03	0.03	4.57	−0.24	−0.03	0.03
CO	5.11	0.31	−0.36	0.36	5.16	0.30	−0.35	0.35	5.14	0.33	−0.35	0.35
CO_2	4.72	−0.08	−0.04	0.04	4.70	−0.15	−0.05	0.05	4.69	−0.12	−0.05	0.05
OH	4.05	−0.76	−0.59	0.59	4.06	−0.79	−0.58	0.58	4.06	−0.76	−0.58	0.58
H_2O	4.78	−0.02	−0.02	0.02	4.43	−0.43	0.00	0.00	4.31	−0.51	0.00	0.00

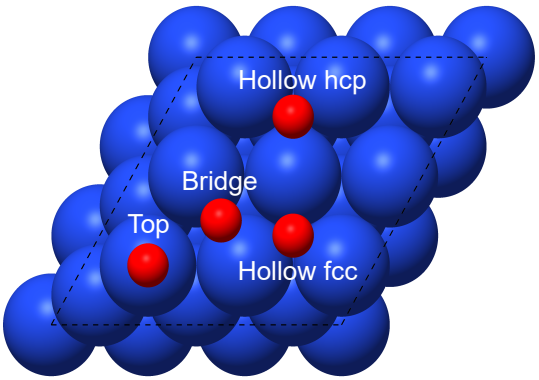

Figure S8: High symmetry adsorption sites (red spheres) on the Cu(111) surface. Blue spheres represent Cu atoms.

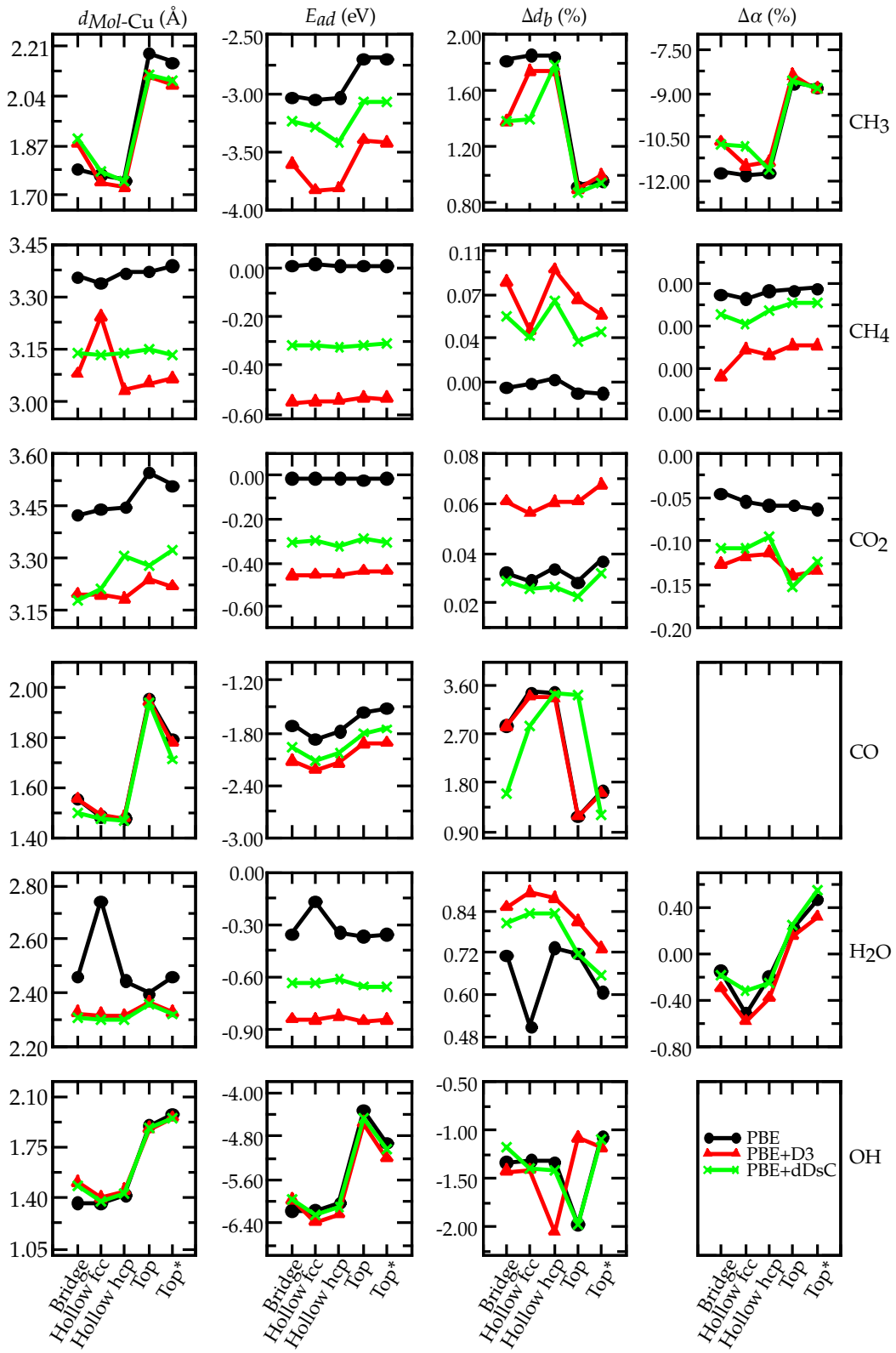

Figure S9: Effect of the vdW corrections on the adsorption properties of CH_3, CH_4, CO_2, CO, CO_2, OH and H_2O on the Cu(111) surface adsorption sites.

References

1 Hohenberg, P.; Kohn, W. Inhomogeneous Electron Gas. *Phys. Rev.* **1964**, *136*, B864–B871, DOI: 10.1103/physrev.136.b864.

2 Kohn, W.; Sham, L. J. Self-Consistent Equations Including Exchange and Correlation Effects. *Phys. Rev.* **1965**, *140*, A1133–A1138, DOI: 10.1103/physrev.140.a1133.

3 Klimeš, J.; Michaelides, A. Perspective: Advances and Challenges in Treating van der Waals Dispersion Forces in Density Functional Theory. *J. Chem. Phys.* **2012**, *137*, 120901, DOI: 10.1063/1.4754130.

4 Grimme, S. Semiempirical GGA-Type Density Functional Constructed with a Long-range Dispersion Correction. *J. Comput. Chem.* **2006**, *27*, 1787–1799, DOI: 10.1002/jcc.20495.

5 Chai, J.-D.; Head-Gordon, M. Long-range Corrected Hybrid Density Functionals with Damped Atom-atom Dispersion Corrections. *Phys. Chem. Chem. Phys.* **2008**, *10*, 6615–6620, DOI: 10.1039/B810189B.

6 Grimme, S.; Antony, J.; Ehrlich, S.; Krieg, H. A Consistent and Accurate ab Initio Parametrization of Density Functional Dispersion Correction (DFT-D) for the 94 Elements H – Pu. *J. Chem. Phys.* **2010**, *132*, 154104, DOI: 10.1063/1.3382344.

7 Grimme, S.; Ehrlich, S.; Goerigk, L. Effect of the Damping Function in Dispersion Corrected Density Functional Theory. *J. Comput. Chem.* **2011**, *32*, 1456–1465, DOI: 10.1002/jcc.21759.

8 Tkatchenko, A.; Scheffler, M. Accurate Molecular van Der Waals Interactions From Ground-state Electron Density and Free-atom Reference Data. *Phys. Rev. Lett.* **2009**, *102*, 073005, DOI: 10.1103/physrevlett.102.073005.

9 Tkatchenko, A.; DiStasio, R. A.; Car, R.; Scheffler, M. Accurate and Efficient Method for Many-Body van der Waals Interactions. *Phys. Rev. Lett.* **2012**, *108*, 236402, DOI: 10.1103/physrevlett.108.236402.

10 Bučko, T.; Lebègue, S.; Hafner, J.; Ángyán, J. G. Improved Density Dependent Correction for the Description of London Dispersion Forces. *J. Chem. Theory Comput.* **2013**, *9*, 4293–4299, DOI: 10.1021/ct400694h.

11 Bučko, T.; Lebègue, S.; Ángyán, J. G.; Hafner, J. Extending the Applicability of the Tkatchenko-Scheffler Dispersion Correction via Iterative Hirshfeld Partitioning. *J. Chem. Phys.* **2014**, *141*, 034114, DOI: 10.1063/1.4890003.

12 Steinmann, S. N.; Corminboeuf, C. A Generalized-gradient Approximation Exchange Hole Model for Dispersion Coefficients. *J. Chem. Phys.* **2011**, *134*, 044117, DOI: 10.1063/1.3545985.

13 Steinmann, S. N.; Corminboeuf, C. Comprehensive Benchmarking of a Density-dependent Dispersion Correction. *J. Chem. Theory Comput.* **2011**, *7*, 3567–3577, DOI: 10.1021/ct200602x.

14 Adamo, C.; Barone, V. Toward Realiable Density Functional Methods Without Ajustable Parameters: The PBE0 Model. *J. Chem. Phys.* **1999**, *110*, 6158.

15 Casimir, H. B. G.; Polder, D. *Phys. Rev. B* **1948**, *73*, 360.

16 Axilrod, B. M.; Teller, E. *J. Chem. Phys.* **1943**, *11*, 299–300.

17 Muto, Y. Force Between Nonpolar Molecules. *Proc. Phys. Math. Soc. Japan* **1943**, *17*, 629–631.

18 Bultinck, P.; Van Alsenoy, C.; Ayers, P. W.; Carbó-Dorca, R. Critical analysis and extension of the Hirshfeld atoms in molecules. *J. Chem. Phys.* **2007**, *126*, 144111, DOI: 10.1063/1.2715563.

19 Becke, A. D.; Johnson, E. R. Exchange-hole dipole moment and the dispersion interaction revisited. *J. Chem. Phys.* **2007**, *127*, 154108, DOI: 10.1063/1.2795701.

20 Tang, K. T.; Toennies, J. P. An improved simple model for the van der Waals potential based on universal damping functions for the dispersion coefficients. *J. Chem. Phys.* **1984**, *80*, 3726–3741, DOI: 10.1063/1.447150.

21 Straumanis, M. E.; Yu, L. S. Lattice Parameters, Densities, Expansion Coefficients and Perfection of Structure of Cu and of Cu – In α Phase. *Acta Crystallogr. A* **1969**, *25*, 676–682, DOI: 10.1107/S0567739469001549.

22 Young, D. A. CHAPTER 13. The Transition Metals. In *Phase Diagrams of the Elements*; University of California Press: Ewing, NJ, USA, 2020; pp 168–195, DOI: 10.1525/9780520911482-014.

23 Rumble, J. R. *CRC Handbook of Chemistry and Physics, 102nd Edition (Internet Version 2021)*; CRC Press/Taylor & Francis, 2021.

24 Freund, L. B.; Suresh, S. *Thin Film Materials: Stress, Defect Formation and Surface Evolution*; Cambridge University Press: Cambridge, England, UK, 2004; DOI: 10.1017/CBO9780511754715.

25 Ledbetter, H. M. Sound Velocities and Elastic-constant Averaging for Polycrystalline Copper. *J. Phys. D: Appl. Phys.* **1980**, *13*, 1879–1884, DOI: 10.1088/0022-3727/13/10/017.

26 de Boer, F. R.; Mattens, W. C. M.; Boom, R.; Miedema, A. R.; Niessen, A. K. *Cohesion in Metals: Transition Metal Alloys*; Cohesion and structure; North-Holland, 1988.

27 Michaelson, H. B. The Work Function of the Elements and Its Periodicity. *J. Appl. Phys.* **1977**, *48*, 4729–4733, DOI: 10.1063/1.323539.

28 Johnson, R. D. NIST Computational Chemistry Comparison and Benchmark Database, NIST Standard Reference Database Number 101 Release 21. 2020; http://cccbdb.nist.gov/.